
Supporting Information for:

A dye-sensitized visible light photocatalyst-Bi₂₄O₃₁Cl₁₀

*Liang Wang¹, Jun Shang¹, Weichang Hao^{*1,2}, Shiqi Jiang¹, Shiheng Huang¹, Tianmin Wang¹, Ziqi Sun², Yi Du^{*2}, Shixue Dou², Tengfeng Xie³, Dejun Wang³ and Jiaou Wang⁴*

¹Center of Materials Physics and Chemistry and Department of Physics, Beihang University, Beijing 100191, P. R. China. ² Institute for Superconducting and Electronic Materials, University of Wollongong, Wollongong NSW 2522, Australia. ³ College of Chemistry, Jilin University, Changchun 130012, P. R. China. ⁴Beijing Synchrotron Radiation Facility, Institute of High Energy Physics, Chinese Academy of Sciences, Beijing 100049, P. R. China.

* Correspondence and requests for materials should be addressed to W. C. H. (email: whao@buaa.edu.cn) or Y. D. (email: ydu@uow.edu.au)

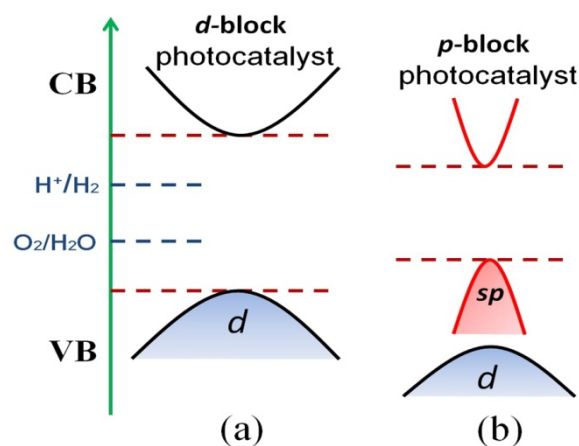


Figure S1. Justification of new strategy for exploring novel visible-light photocatalysts in *p*-block compounds.

As shown in Figure S1(a), conventional *d*-block photocatalysts have a wide band gap with a relatively flat valence band (VB) and relatively flat conduction band (CB). Therefore, their visible-light photocatalytic properties are hindered by low photon absorption and ineffective photoinduced electron-hole pair separation under visible light. The novel *p*-block photocatalysts proposed in this work possess more dispersive electronic structures with narrow band gaps (Figure S1(b)), which prompt absorption of visible light as well as separation of photoinduced charge carriers. Hence, *p*-block compounds are more suitable as parent materials for high-efficiency visible-light photocatalysts in comparison with *d*-block compounds.

To confirm the idea of exploring visible light photocatalysts by using only *p*-block elements, $\text{Bi}_{24}\text{O}_{31}\text{Cl}_{10}$ powders were synthesized using a simple chemical precipitation method. The structural parameters, morphology, and effects of the post-annealing temperature on the structure were determined through scanning electron microscopy (SEM) and X-ray diffraction (XRD). The XRD pattern shows that the $\text{Bi}_{24}\text{O}_{31}\text{Cl}_{10}$ sample is single phase with lattice parameters $a = 9.99 \text{ \AA}$, $b = 3.97 \text{ \AA}$, and $c = 6.72 \text{ \AA}$. With increasing temperature, the intensity of the XRD peak increases, and the full width at half-maximum of the diffraction peak narrows simultaneously, which further supports the particle sizes observed in the SEM images. It is noteworthy that $\text{Bi}_{24}\text{O}_{31}\text{Cl}_{10}$ retains its

crystal structure, and no impurity diffraction peak appears, even up to 800 °C, which indicates that $\text{Bi}_{24}\text{O}_{31}\text{Cl}_{10}$ is thermally stable. The SEM images show that the $\text{Bi}_{24}\text{O}_{31}\text{Cl}_{10}$ grains grow larger with increasing annealing temperature. Meanwhile, agglomeration is observed when the temperature is higher than 700 °C. The SEM images show that the particles are plate-like, with diameters of several hundred nanometers and thicknesses of 50-100 nm.

We found that the optimum annealing temperature is 600 °C, which is evidenced by the best catalytic performance, as shown in Figure S3.

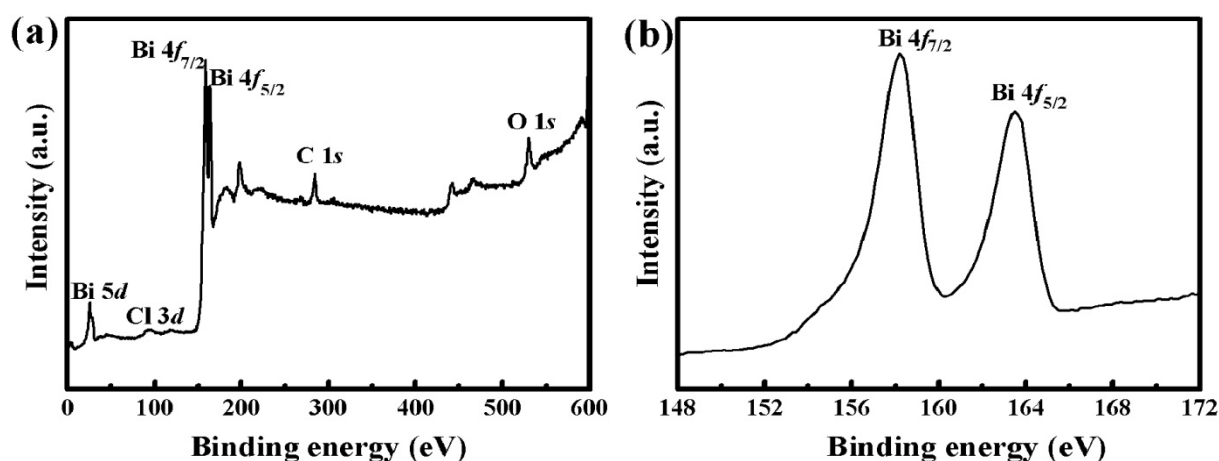


Figure S2. XPS spectra for $\text{Bi}_{24}\text{O}_{31}\text{Cl}_{10}$: (a) survey spectrum and (b) Bi 4f.

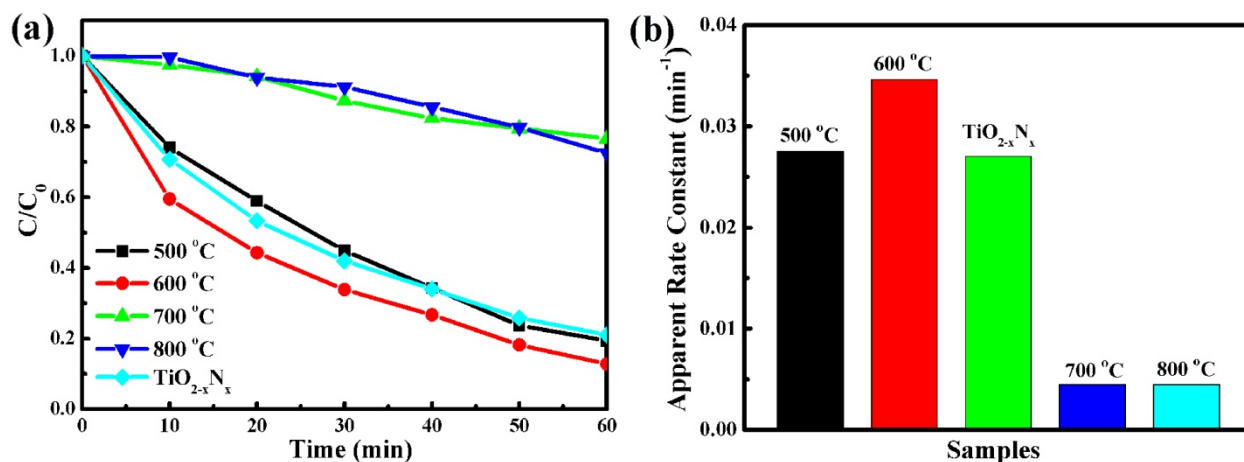


Figure S3. (a) Comparison of the visible light photocatalytic activity of $\text{Bi}_{24}\text{O}_{31}\text{Cl}_{10}$ submicron platelets post-annealed at different temperatures with that of N-doped TiO_2 nanocrystals. (b) Apparent rate constants of different samples.

In order to determine whether the RhB undergoes a process of complete degradation or a de-coloring process, the removal of total organic carbon (TOC) was chosen as a mineralization index to characterize the RhB degradation. The time independence of the TOC data in the RhB solution in the presence of the $\text{Bi}_{24}\text{O}_{31}\text{Cl}_{10}$ catalyst under visible-light irradiation is shown in Figure S4. It was observed that 42% of the TOC was eliminated after 105 min of irradiation, indicating that RhB could be mineralized in this process.

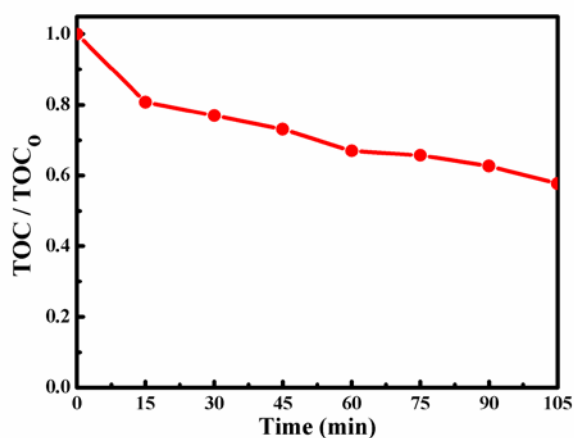


Figure S4 TOC removal in the presence of $\text{Bi}_{24}\text{O}_{31}\text{Cl}_{10}$, with an initial RhB concentration of 0.02 mmol/L and catalyst dosage of 1 g/L under visible light irradiation.

The durability and stability of the $\text{Bi}_{24}\text{O}_{31}\text{Cl}_{10}$ were characterized by a cycling test of photodegradation, in which $\text{Bi}_{24}\text{O}_{31}\text{Cl}_{10}$ demonstrated high photocatalytic activity over five runs, as shown in Figure S5. XRD patterns of $\text{Bi}_{24}\text{O}_{31}\text{Cl}_{10}$ collected before and after photodegradation indicate that this compound is very stable during the photocatalytic process, as shown in Figure S6.

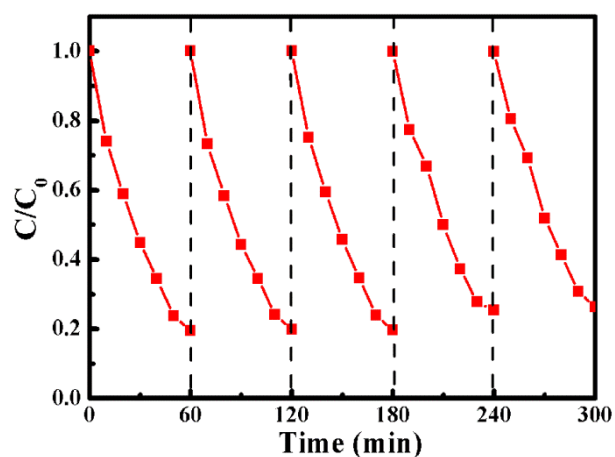


Figure S5. Cycling test of visible-light photocatalytic activity.

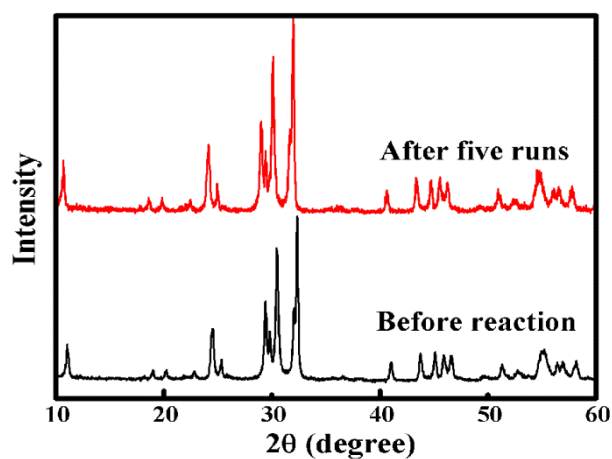


Figure S6. XRD patterns of $\text{Bi}_{24}\text{O}_{31}\text{Cl}_{10}$ before and after photodegradation.

Figure S7 shows the transmittance spectrum of a monochromatic light filter with the pass wavelength of 550 nm, which was used in the experiments discussed in the main text.

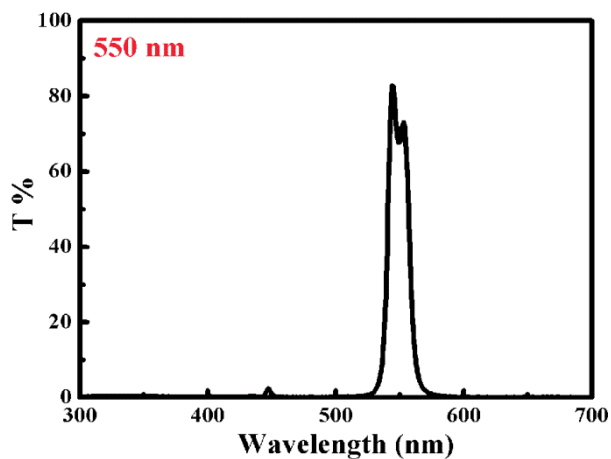


Figure S7. Transmittance spectrum of 550 nm cut-off filter.

The $\text{Bi}_{24}\text{O}_{31}\text{Cl}_{10}$ can be sensitized by the dye N719 because the excited state of N719 (-0.71 V vs. NHE) is more negative than the conduction band of the $\text{Bi}_{24}\text{O}_{31}\text{Cl}_{10}$, as indicated by the schematic diagram in Figure S8.

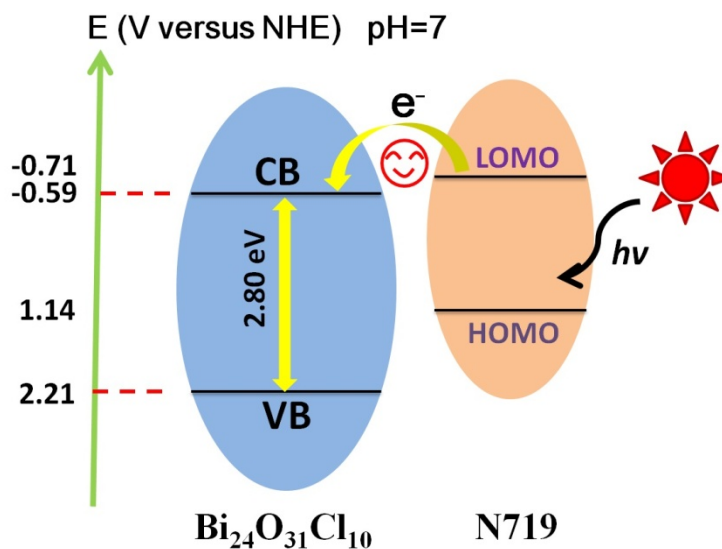


Figure S8. Schematic diagram of estimated band positions of $\text{Bi}_{24}\text{O}_{31}\text{Cl}_{10}$ and N719, as well as the possible transport pathway of photoinduced electrons on N719.